Astron. Astrophys. 293, 240–251 (1995)

ASTRONOMY AND ASTROPHYSICS

# Infrared lines as probes of solar magnetic features

## IX. Mg I 12 $\mu$m diagnostics of solar plage

**J.H.M.J. Bruls*** **and S.K. Solanki**

Institut für Astronomie, ETH-Zentrum, CH-8092 Zürich, Switzerland

Received 26 August 1993 / Accepted 6 November 1993

**Abstract.** The Mg I 12.32 $\mu$m line is a prime diagnostic for studying upper photospheric magnetic fields on the Sun. We study for the first time its behavior using flux-tube models with magnetic field strengths and filling factors characteristic of solar plage in order to establish the line's capabilities for measuring plage magnetic fields.

We show that this line is only moderately sensitive to the range of temperatures expected for solar plages, including the chromospheric temperature rise. This low sensitivity considerably enhances this line as a magnetic field diagnostic for the upper photosphere of plages.

We find that besides being highly sensitive to the field strength in flux tubes, the shape and Zeeman splitting of this line are almost equally sensitive to the magnetic filling factor at the flux-tube base. This combined sensitivity leads to the large range of profile shapes observed in plages. Not only can the 12 $\mu$m emission lines be used to determine the sub-spatial-resolution distribution of flux-tube field strengths, but also the sub-spatial-resolution distribution of filling factors (i.e. they can provide an estimate of the "clumpiness" of the flux-tube distribution on a small scale).

We also provide evidence that simple two-component modeling of magnetic flux tubes, without taking into account the height-dependence of the flux-tube size, may lead to erroneous conclusions in the case of the Mg I 12 $\mu$m lines, and that at least 1.5-D computations are required to adequately model these lines in magnetic flux tubes.

Computations also show that standard flux-tube models simultaneously reproduce the observed splitting of the $g = 3$ Fe I lines at 1.5648 $\mu$m (formed in the low photosphere) and at 525.02 nm (middle photosphere), as well as of the 12.32 $\mu$m emission line (upper photosphere). Our computations thus support the currently standard view that solar plages are composed of flux tubes with kGauss fields in the lower and mid photosphere, and that the thin-tube approximation is an adequate representation of the magnetic stratification in these flux tubes.

*Send offprint requests to*: S.K. Solanki

* *Present address:* Instituto de Astrofisica de Canarias, c/ Via Lácta s/n, E-38200 La Laguna, Spain

**Key words:** Sun: infrared – Sun: chromosphere – Sun: faculae, plages – Sun: magnetic fields – Sun: photosphere

### 1. Introduction

The Mg I 12 $\mu$m lines, although quite weak, are formed in the upper photosphere and for the first time enable the measurement of intrinsic magnetic field strengths as low as 200 G directly from their Zeeman splitting (cf. Bruls et al. 1994). Their large Zeeman sensitivity and favorable formation height have made the Mg I 12 $\mu$m lines the most important diagnostic of magnetic fields in the upper photosphere. They have been used to observationally study sunspot penumbrae, and solar plage and magnetic network fields (Brault & Noyes 1983; Deming et al. 1988b, 1990; Zirin & Popp 1989; Hewagama 1991; Hewagama et al. 1993). In paper VIII of the present series (Bruls et al. 1994) we considered the diagnostic potential of the 12 $\mu$m lines for the study of sunspot penumbrae. In the present paper we concentrate on uncovering the capabilities of these lines to determine the magnetic field in the upper photospheric layers of solar plage.

Solar plage and network regions are thought to consist of a large number of individual small magnetic flux tubes, surrounded by field-free material. The flux tubes fill only a fraction of the surface area at photospheric heights. Pressure equilibrium between the flux tubes (internal gas pressure and magnetic pressure) and their environment (external gas pressure) requires that the flux tubes fan out with height; eventually they merge into a magnetic canopy. For filling factors characteristic of active regions the merging height corresponds to about the formation height of the Mg I 12 $\mu$m lines (Solanki & Steiner 1990). This property greatly influences the line profile shapes.

Although it is often thought that the profiles of fully Zeeman split lines are straightforward to interpret, the complex shapes of the 12 $\mu$m profiles observed in solar plages, belie this (e.g. Zirin & Popp 1989). Solar plages are not the simple, regular structures suggested by two-component models.

Zeeman-insensitive lines are quite adequately reproduced by two-component models, but already the Fe I 1.5648 $\mu$m $g = 3$ line required flux-tube models (Zayer et al. 1989) and sometimes multiple field-strength components in the resolution element (Rüedi et al. 1992, Paper III) to be reproduced. The 12 $\mu$m lines are even more sensitive to the detailed composition of the plage magnetic field, since their line shapes not only depend on the mixture of field strengths in the resolution element, but also on the distribution of filling factors, i.e. on the way the magnetic flux tubes are distributed over the solar surface. In order to interpret and understand plage profiles there is no alternative to detailed modeling. This is particularly so, since the diffraction limit of even the largest current solar telescope corresponds to an area on the solar surface that is considerably larger than a typical flux tube. Therefore, the observed line profiles are averages over many individual flux tubes.

After discussing the input data and computational technique in Sect. 2, we synthesize Stokes $I$ and $V$ profiles of the Mg I 12.32 $\mu$m line in plage regions, and study the sensitivity to photospheric and chromospheric temperature variations (Sect. 3.1), magnetic filling factors (Sect. 3.2) and magnetic field strengths (Sect. 3.3). We compare with results obtained from visible (525.02 nm) and near-infrared (1.5648 $\mu$m) Fe I lines in Sect. 3.4, and discuss the validity of scaling line profiles from two-component modeling in Sect. 3.5. We end this paper with a discussion of the diagnostic value of the 12.32 $\mu$m line in Sect. 4.

## 2. Input data, models and radiative transfer computations

### 2.1. The Mg model atom

The basic Mg I atomic data for this plage flux-tube investigation are from the non-LTE (local thermodynamic equilibrium) Mg I 12 $\mu$m line formation analysis by (Carlsson et al. 1992), who produce the observed quiet-Sun Mg I 12 $\mu$m line profiles without ad hoc assumptions. The small corrections to the model atom data, described in Paper VIII, were taken into account.

Both Mg I 12 $\mu$m lines have complex but still fairly regular splitting patterns (e.g. Fig. 1 of Paper VIII) since they are in the Paschen-Back regime for typical solar magnetic field strengths, but Chang (1987) and Hewagama (1991) have shown that to high accuracy they can be represented by a simple Zeeman triplet with effective Landé factor unity. The additional splitting due to atomic fine structure, independent of the magnetic field strength, amounts to about 1 mK ($10^{-3}$ cm$^{-1}$), which is much smaller than the thermal broadening of the line profiles. Only at very low field strengths, at which the $\sigma$- and $\pi$-components overlap, must corrections to this pattern be taken into account. Although we compute only the 12.32 $\mu$m line, the present results should also be valid for the 12.22 $\mu$m line, due to the similarity of the two lines.

### 2.2. The Fe model atom

For comparison with the Mg I profiles some profiles of the Fe I lines at 525.02 nm and 1.5648 $\mu$m are computed. Since these Fe I lines are formed relatively deep in the photosphere, deviations from LTE are expected to be small. We nevertheless compute the non-LTE statistical equilibrium employing an updated version of the 100-level iron model atom presented by Watanabe & Steenbock (1986) and Gigas (1986). The oscillator strengths of the lines in the iron model atom have been updated using the compilation by Fuhr et al. (1988). Only minor changes in the model atom were required to incorporate the high-excitation infrared line in the atom, the oscillator strength of which was derived from Solanki et al. (1992a), Paper II of the present series, assuming the meteoritic iron abundance of $3.2 \times 10^{-5}$ ($\log N_{\rm Fe} = 7.51$ on the $\log N_{\rm H} = 12$ scale; Anders & Grevesse 1989). The original electron collision cross-sections have been adopted, whereas neutral particle collisions have been neglected on the premise that they play a minor role in thermalizing the already LTE-like excitation equilibrium of neutral iron in the photosphere.

### 2.3. Atmospheric and magnetic models

We use axially-symmetric two-component atmospheric models, composed of a magnetic flux tube embedded in a non-magnetic atmosphere. The non-magnetic atmosphere surrounding the flux tube is represented by the quiet-Sun model of Maltby et al. (1986) We use flux-tube models PLA (without chromospheric temperature rise), PC1, PC2, PC3 and NC2 of Bruls & Solanki (1993). Plage flux-tube models PC1, PC2 and PC3 have a chromospheric temperature rise similar to that of the Maltby et al. (1986) quiet-Sun model attached at continuum optical depths $\tau_{500}$ of about $10^{-4.0}$, $10^{-3.5}$ and $10^{-2.5}$, respectively. At the onset of the chromospheric temperature rise the exponential decrease with height of the electron density is interrupted by a gradual order of magnitude increase over a layer of a few scale heights thickness, above which an exponential decrease is resumed. Solar network flux-tube model NC2 has the same chromosphere as PC2, but is appreciably hotter in the photosphere. The temperature stratification of these models is shown in the top panel of Fig. 2. The radial expansion of the flux tubes with height, i.e. the increase of the magnetic filling factor with height and the associated proportional decrease of the magnetic field strength (flux conservation), is computed by means of the "thin-tube" approximation (Defouw 1976; Schüssler 1986), which neglects all lateral variation of parameters within the flux tubes. For not too large flux tubes the thin-tube approximation provides good agreement with more general solutions of the magnetohydrodynamic equations (Knölker & Schüssler 1988; Steiner & Pizzo 1989). We also find that this is true for the merging height (see below) from comparisons with the computations of Solanki & Steiner (1990).

In addition to the field strength $B_0$ at the $z = 0$ level (corresponding to $\tau_{500} = 1$ in the quiet Sun) we also prescribe the filling factor $f_0$ at that height. The flux tube is only allowed to expand up to the height at which the cross-sectional area becomes $1/f_0$ times as large as its area at $z = 0$. At this height, $z_{\rm m}$, the flux tube is assumed to merge with its nearest neighbors. Some smoothing has been applied to the field strength and flux-

tube radius stratification. This not only removes fluctuations in the field strength produced by numerical inaccuracies, but also mimics some effects due to magnetic tension. It is important to keep in mind that $z_m$ decreases as $f_0$ increases and that the field strength above $z_m$ is constant and has the value $B_m = f_0 \times B_0$, i.e. it depends equally on the field strength and the filling factor in the low photosphere. $B_m$ is important for the present study because it influences the line profile of the 12.32 $\mu$m line. We use a grid of models with magnetic filling factors of $f_0$ = 1, 2, 4, 8, 16 and 32%, and magnetic field strengths of $B_0$ = 500, 1000, 1400, 1600 and 1680 G. The boundaries of the computed flux tubes are indicated in Fig. 3.

### *2.4. Radiative transfer computations*

The statistical equilibrium and radiative transfer equations are solved in 1-D fashion for 10 representative vertical rays through each flux-tube model at different distances from the flux-tube axis, distributed such that they cross the flux-tube boundary at regularly spaced heights. This way of distributing the rays generally accomplishes a good sampling of the whole flux-tube structure (Solanki & Roberts 1992), although for very low magnetic filling factors a larger number of rays may be required to reduce inaccuracies. All computations simulate vertical flux tubes situated at solar disk center. The statistical equilibrium and radiative transfer equations are solved neglecting the magnetic field. We employ version 2.0 of Carlsson's (1986) radiative transfer code MULTI, with the Olson et al. (1986) local operator to cope with the large number of levels and lines in the Mg I model atom, and with an improved opacity treatment added. Updated neutral metal opacities (Mathisen 1984) have been introduced in the original opacity package of MULTI version 1.0 (adopted from Auer et al. 1972), and wavelength-dependent fudge factors, empirically determined from quiet-Sun disk-center continuum-intensity fits, have been applied to these opacities in order to simulate the ultraviolet "line haze" (cf. Bruls 1992, Paper VIII).

The computed line source functions and opacities are used as input for the Diagonal Element Lambda Operator (DELO) Stokes profile synthesis code (Rees et al. 1989; Murphy & Rees 1990; Murphy 1990) to compute Zeeman-split Stokes $I$ and $V$ profiles for each ray, accounting properly for the pertinent magnetic field stratification. Relying on the field-free approximation, which has been shown to be accurate (Rees 1969; Rees 1987), the introduction of the magnetic field is assumed not to influence the statistical equilibrium. Finally, the average line profile is computed, taking into account the proper weight of each ray.

## 3. Results

### *3.1. Temperature sensitivity*

Several studies exist of the photospheric temperature stratification in plage flux tubes (e.g. Chapman 1979; Solanki 1986; Walton 1987; Keller et al. 1990; Solanki & Brigljević 1992). These are LTE analyses of magnetically sensitive lines in the visible. Their LTE assumption breaks down in the upper photosphere, where the line source functions start to deviate from the Planck function due to photon losses, so that excitation temperatures rather than electron temperatures are obtained. Also a few non-LTE analyses exist (Stenholm & Stenflo 1977; Ayres et al. 1986; Solanki & Steenbock 1988; Solanki et al. 1991), but they concentrate on Stokes $I$ profiles, which are very sensitive to various parameters of the non-magnetic atmosphere as well. A first attempt to model the upper layers of flux tubes from observed Stokes $V$ profiles without the assumption of LTE was undertaken by Bruls & Solanki (1993)[1]. The conclusion of that paper was that the chromospheric temperature rise in plage and network flux tubes starts 200 to 300 km deeper than in the quiet-Sun model, but the exact height also depends on the initial steepness of the rise. Due to this uncertainty we start with a demonstration of the relative insensitivity of the 12.32 $\mu$m line to chromospheric and photospheric temperature changes in the flux-tube models. A uniform longitudinal magnetic field of 500 G is assumed to be universally present, i.e. the magnetic filling factor is unity. Constant magnetic field strength throughout the atmosphere is usually an unrealistic assumption, but here it simplifies the analysis since it prohibits differences in line splitting that could otherwise result from different line formation heights (with associated magnetic field strength differences) for the various flux-tube models.

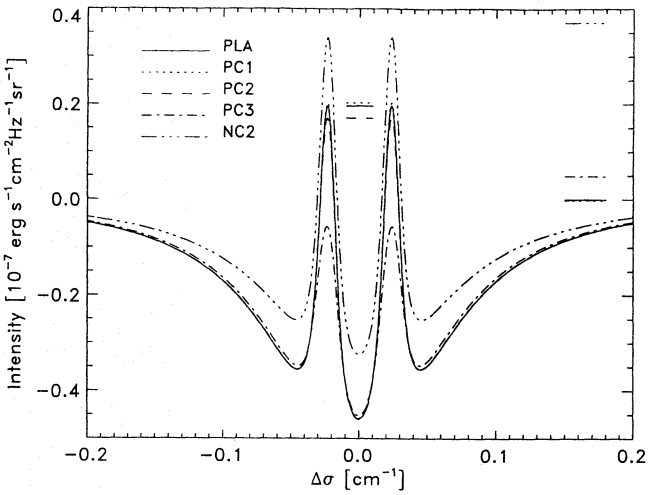


**Fig. 1.** Mg I 12.32 $\mu$m line profiles for plage flux-tube models with different chromospheric temperatures and for one network flux-tube model, which is about 700 K hotter in the photosphere. A uniform longitudinal magnetic field of 500 G is assumed for all models. The close-lying peak intensities of PLA, PC1 and PC2 are indicated by horizontal lines between the $\sigma$ peaks. The continuum intensities have been subtracted from each profile to exhibit the profile similarities more clearly, but their values relative to the PLA continuum intensity are indicated by the horizontal lines at right

[1] Stenholm & Stenflo (1978) had previously calculated Stokes $V$ profiles in flux tubes using two-level atoms, but they were mainly interested in horizontal transfer effects in the deeper layers of flux tubes.

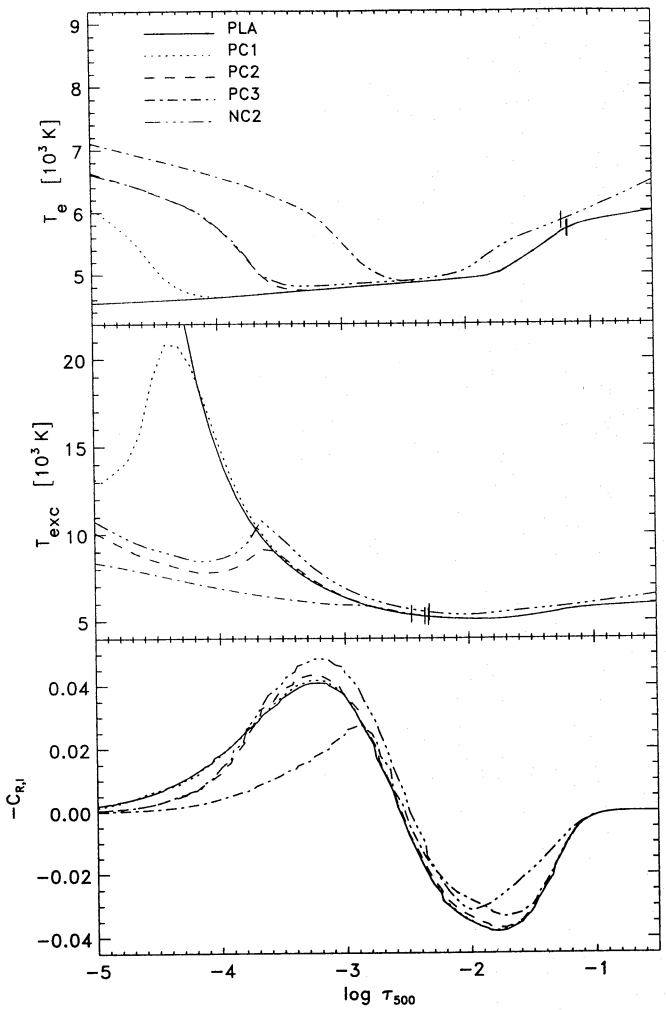


**Fig. 2.** *Top:* Electron temperatures vs. log $\tau_{500}$. The tickmarks indicate 12 $\mu$m continuum optical depth unity. *Middle:* Excitation temperatures derived from the computed 12.32 $\mu$m line source functions. The tickmarks indicate line center optical depth unity for the Zeeman unsplit line. Optical depth unity at the $\sigma$-peak wavelengths of the Zeeman split line is located slightly deeper. *Bottom:* Stokes $I$ emission (negative line depression) contribution functions $-C_{R,I}$ for a wavelength representative of the $\sigma$ peaks in the line profiles of Fig. 1

Figure 1 displays Stokes $I$ profiles for four plage flux-tube models (PLA, PC1, PC2, PC3) with different options for the chromospheric temperature rise, and network flux-tube model NC2. The variation of the 12 $\mu$m continuum intensities is very small: for models PLA, PC1 and PC2 they are the same to within 0.05%; it is 0.5% larger for PC3, and 4% larger for NC2. For a deeply located onset of the chromospheric temperature rise (model PC3) the tail of the intensity contribution function (CF) in the upper atmosphere samples part of the chromospheric rise of the continuum source function (see Fig. 7 of Carlsson et al. 1992), which is equal to the Planck function (Fig. 2, top panel), so that larger emergent continuum intensities result. The increase of the NC2 continuum intensities stems from the larger photospheric temperatures.

The 12.32 $\mu$m line emission weakens for a chromospheric temperature rise that starts deep in the flux tube. That results from the behavior of the ionization and excitation equilibrium with changing temperature $T_e$ and electron density $N_e$. The actual non-LTE populations of the neutral and ionized stages do not follow chromospheric $T_e$ changes, because they are mainly set by the photospheric ultraviolet radiation fields and by the collective line photon losses in the Rydberg lines. The Saha-Boltzmann equilibrium (LTE) reference populations, however, depend sensitively on $T_e$ through the Boltzmann factor $\exp(-E_{exc}/kT_e)$, so that the state of overionization that generally exists near the temperature minimum — the equivalent black body radiation temperature $T_{rad}$ of the ionizing ultraviolet radiation exceeds the local electron temperature $T_e$ — rapidly changes into underionization ($T_{rad} < T_e$) when $T_e$ increases in the chromosphere. The associated increase of $N_e$ affects the LTE reference ionization equilibrium stronger than the actual non-LTE ionization equilibrium, because the latter is also determined by infrared line photon losses. Due to the overpopulation of the lower levels of the neutral stage and the increased collisional coupling between the Rydberg levels, the population departure differences between the Rydberg levels, which are caused by photon losses in the infrared Rydberg lines, are smaller than without chromospheric $T_e$ and $N_e$ enhancements. Consequently, the 12.32 $\mu$m line source function is less enhanced over the Planck function. This is visible in the middle panel of Fig. 2 as a slower increase or even a decrease of the excitation temperature $T_{exc}$ (equivalent to the 12.32 $\mu$m line source function) with height. The overall 12.32 $\mu$m line source function change, relative to the situation without a $T_e$ rise, increases with deeper onset of this rise. The increase of $N_e$ at the onset of the chromosphere, however, causes a dip in $T_{exc}$ that decreases in strength with deeper location: a tenfold increase of the collisional rates has larger impact in higher layers where the importance of infrared line photon losses in setting the departure coefficient differences is smaller.

The bottom panel of Fig. 2 summarizes the 12.32 $\mu$m line formation in the form of (relative) line emission (negative line depression) CFs for Stokes $I$, $-C_{R,I}$. It shows $-C_{R,I}$ representative of the $\sigma$-peak wavelengths. The positive part of the CF curves represents the line emission, which is partly or completely canceled by the absorption part deeper in the atmosphere. The emission coming from the very top of the atmosphere decreases with increasing strength of the chromosphere; the drop of the CFs initially steepens with increasing strength of the chromosphere due to the decrease of the line source function. For model PC3 the sharp drop in particle densities pushes the line formation height significantly down.

Figure 1 shows larger intensities all over the line profile for model NC2. The difference with the profile for model PC2, that remains after subtracting the continuum intensities, is due to the larger line source function of model NC2 (middle panel of Fig. 2). In the photosphere ($\tau_{500} \gtrsim 10^{-2}$) the hotter ultraviolet radiation causes larger overionization, i.e. larger population departure differences among the Rydberg levels, so that the line source function to Planck function ratio is enhanced. Addition-

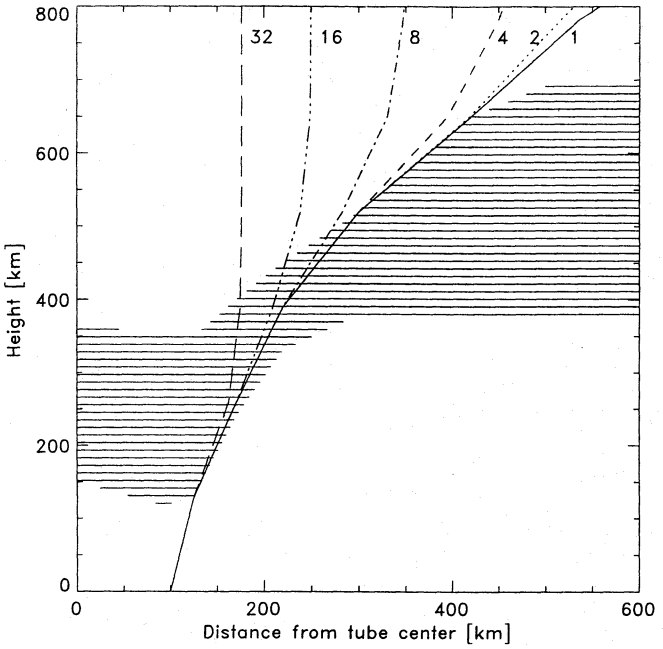


**Fig. 3.** Flux-tube geometry for different magnetic filling factors indicated at the top in percent. All flux tubes have been given a radius of 100 km at $z = 0$ ($\tau_{500} = 1$ in the surrounding quiet-Sun atmosphere). The flux tube with the highest filling factor merges with a neighboring tube at a height of only $\approx$ 300 km, whereas the ones with the lowest filling factors have not yet reached their maximum radius at a height of 800 km. The shaded area indicates the approximate formation region of the emission part of the Mg I 12.32 $\mu$m line. The plotted "flux-tube boundary" is simply a linear interpolation between the points of intersection of the individual rays with the true boundary

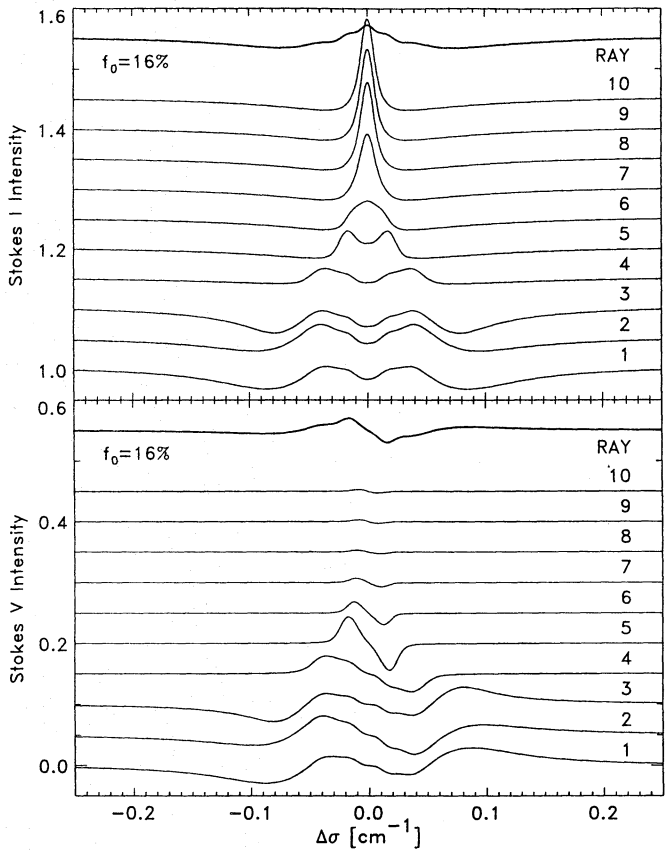


**Fig. 4.** Mg I 12.32 $\mu$m Stokes $I$ (top) and $V$ profiles (bottom) for the 10 vertical rays through the PC2 model with filling factor $f_0 = 16\%$ and $B_0 = 1600$ G. The curves are numbered 1 to 10 from the flux-tube axis to the outermost ray. The uppermost curve is the average line profile. To get a regular spacing of the profiles, all Stokes $I$ and $V$ intensities are normalized to the respective Stokes $I$ continuum intensities, and then shifted upward in steps of 0.05

ally, for model NC2 the Planck function itself is larger than for PC2. Above $\tau_{500} \approx 10^{-2}$ models NC2 and PC2 have (nearly) equal $T_e$, so that only the increased ionization remains; this results in nearly constant source function enhancement over a large height range. Measured from the line-center intensity minimum the NC2 emission peaks are nearly equally strong as for the PC2 line profile, which is mainly due to this constant line source function enhancement over a large height range.

In summary, only for model PC3 does the strength of the emission deviate. Fortunately, Bruls & Solanki (1993) could show that averaged over many flux tubes this model conflicts with observations of the Fe II 492.3 nm line. Consequently, the 12.32 $\mu$m line has an unexpectedly low sensitivity to chromospheric temperature, which enhances its potential for plage magnetic field measurement and modeling, since it should be reasonably independent of the thermal structure of the atmosphere.

### 3.2. *Filling factors*

A sequence of flux-tube models that differ only in their magnetic filling factors (Fig. 3) illustrates that the Mg I 12.32 $\mu$m line profile depends strongly on this parameter, not only in the Stokes $V$ amplitude, but also in the shape of the Stokes $I$ and $V$ profiles. The atmospheric model employed is the PC2 plage model, with magnetic filling factors $f_0$ ranging from 1 to 32%; the magnetic field strength $B_0$ (at $z = 0$) is kept at 1600 G. Stokes $I$ and $V$ profiles formed along individual rays are shown in Fig. 4, for $f_0 = 16\%$. At large distance from the flux-tube axis, the Stokes $I$ profiles are indistinguishable from quiet-Sun profiles. Note that far from the flux-tube axis the shaded region lies almost completely in the non-magnetic atmosphere. The Stokes $V$ profiles (Fig. 4, bottom panel) best reveal that the long chromospheric tail of the contribution function still does reach above the magnetic merging height, where it measures the rather weak height-independent field. Towards the tube

**Table 1.** Comparison between the field strength above the merging height, $B_m$, and the field strength derived from the $\sigma$-peaks of the 12.32 $\mu$m line, $B_A$

| $f_0$ | 1% | 2% | 4% | 8% | 16% | 32% |
|---|---|---|---|---|---|---|
| $B_m = f_0 B_0$ | 16 | 32 | 64 | 128 | 256 | 512 |
| $B_A$ | 205 | 205 | 225 | 245 | 355 | 570 |

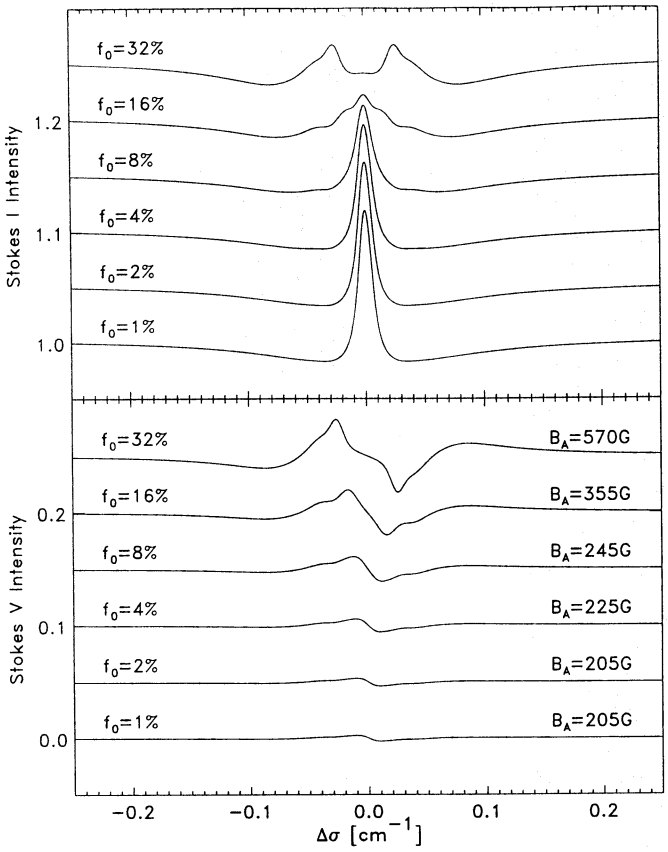


**Fig. 5.** Average Mg I 12.32 $\mu$m Stokes $I$ (top) and $V$ profiles (bottom) for model PC2 with different filling factors $f_0$ (indicated at the left). The apparent magnetic field strengths $B_A$ corresponding to the Stokes $V$ splitting are indicated at the right. The spacing of the line profiles is produced as in Fig. 4

axis the line formation gradually moves into the magnetic zone completely (cf. Fig. 3). The Stokes $I$ profile first broadens and eventually splits up into the two $\sigma$-components (e.g. rays 6 and 5). Still closer to the flux-tube axis (rays 1–4), the large vertical field strength gradients that exist deeper in the atmosphere dominate the profile shape and produce significant broadening of the $\sigma$-peaks.

A wide absorption trough is present (but often barely visible) in Stokes $I$ of all rays. The corresponding Stokes $V$ absorption $\sigma$-components, which can only exist if there are non-zero fields in the photosphere, have opposite sign from the above emission $\sigma$-components and their amplitude is approximately proportional to $B$ — the weak-field approximation is still valid for such wide features. Especially at larger photospheric field strengths (i.e. for rays close to the flux-tube axis) this leads to increasing canceling of Stokes $V$ in the inner line wings.

In the average Stokes $I$ profile (top curve in upper panel of Fig. 4) all parts of the flux-tube model are represented: the line-center emission (from the non-magnetic atmosphere below the canopy), a hint of narrow emission $\sigma$-peaks (from the constant-field canopy) not yet separated from the line-center emission peak, wider and further separated emission $\sigma$-peaks (from the deeper magnetic parts), and the absorption wings (from the entire photosphere). All these features, except the central emission, are also present in the average Stokes $V$ profile (top curve in lower panel of Fig. 4). The line-center emission peak, which dominates the $f_0 \leq 16\%$ Stokes $I$ profiles in Fig. 5, but which is hardly visible in the $f_0 = 32\%$ profiles, is almost entirely non-magnetic in origin, because the magnetic $\pi$-component is very weak due to the almost longitudinal magnetic fields in the line formation region.

Similar behavior as for the above case of $f_0 = 16\%$ is displayed by the average Stokes $I$ and $V$ profiles for other $f_0$-values (Fig. 5). At lower $f_0$ (roughly $f_0 < 8\%$) little or no magnetic signature is directly visible in Stokes $I$ and only a marginal signal is seen in Stokes $V$. With increasing $f_0$ the unpolarized quiet-Sun contribution to the line-center emission peak in Stokes $I$ becomes weaker, and the emission $\sigma$-peaks become visible; first only as a very small intensity enhancement near the deepest points in the Stokes $I$ profile and at $f_0 = 32\%$ as two separated wide peaks. The wide, low part of the $\sigma$-peaks results from the strong photospheric fields with large gradients, and the narrow part closer to line center arises in the nearly constant magnetic field close to the merging height. $B_m$ increases linearly with $f_0$, so that the splitting of the narrow $\sigma$-peaks in Stokes $I$ also increases with $f_0$. The apparent magnetic field strength $B_A$, derived from the Stokes $V$ splitting, corresponds to the field strength at the median formation height of the emission peaks. As can be seen from Table 1, $B_A$ represents an upper limit to $B_m$: at low $f_0$ the line is formed well below the canopy, while at larger $f_0$ values $B_A$ represents the field strength just below the height where it becomes constant. In addition, for small $f_0$ the Stokes $V$ splitting is incomplete, so that $B_A$ is an overestimate of the actual field strength (cf. Fig. 7 of Paper VIII). For $f_0 \gtrsim 5\%$ there is a measurable dependence of $B_A$ on $f_0$, and for $f_0 \gtrsim 16\%$ $B_A$ changes almost as rapidly as $B_m$. The Stokes $V$ amplitude of the emission $\sigma$-peaks increases approximately linearly with $f_0$.

### *3.3. Magnetic field strengths*

Figure 6 displays the dependence of the Mg I 12.32 $\mu$m line profile on $B_0$. The magnetic filling factor $f_0$ is 16% at the left and 32% at the right. $B_A$ increases with $B_0$, but the exact dependence is relatively complex. At small $B_0$, $B_A$ tends to become independent of $B_0$ since the line then enters the weak-field regime and is no longer fully split. At larger $B_0$ the $B_A$ value can change either more or less rapidly than $B_0$, depending on a number of factors. For instance, if $z_m$ is much higher than the formation height of the line, it is $B(\tau_{int}) = 1$ rather than $B_0$ which determines $B_A$ ($\tau_{int}$ is the continuum optical depth in the tube at 500 nm). As shown in Paper II, $B(\tau_{int}) = 1$ increases much more rapidly than $B_0$ for $B_0 \gtrsim 1400$ G, so that $B_A$ is then also expected to change more rapidly than $B_0$. For large filling factors, $f_0 \gtrsim 30\%$, on the other hand, $B_A$ is determined chiefly by $B_m = f_0 B_0$.

In addition, the Stokes $V$ amplitude of the absorption trough, which has the opposite sign of the emission $\sigma$-peaks of Stokes $V$, increases linearly with $B_0$, and its splitting remains

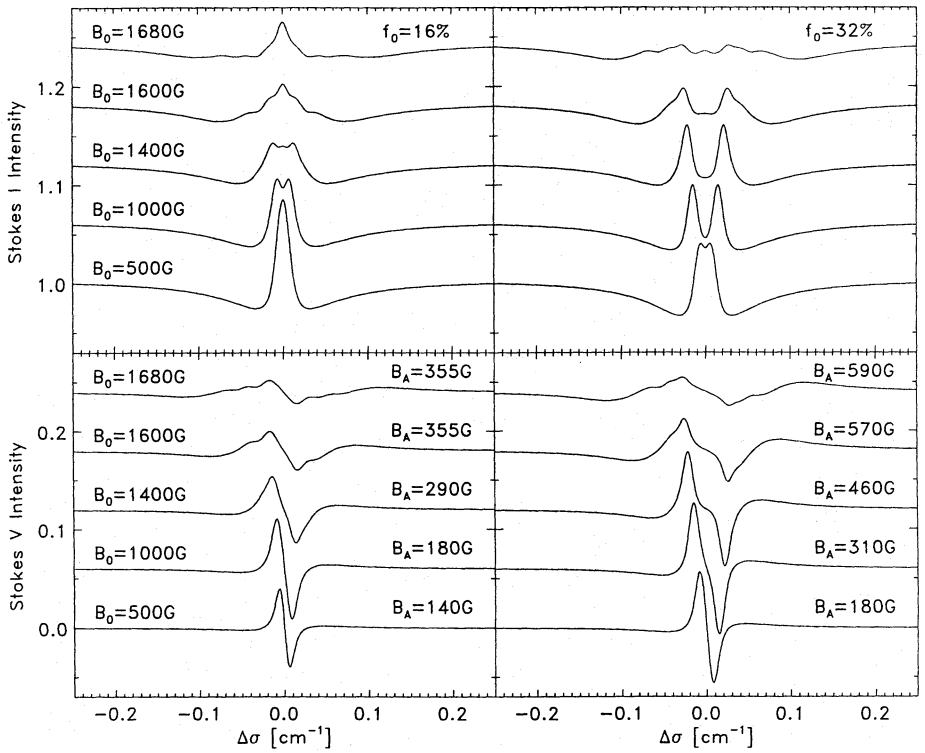


**Fig. 6.** Average Mg I 12.32 $\mu$m Stokes $I$ (top) and $V$ profiles (bottom) for model PC2 with different magnetic field strengths and with filling factors of 16% (left) and 32% (right). To get a regular spacing of the profiles, all Stokes $I$ and $V$ intensities have been normalized to the respective Stokes $I$ continuum intensities, and then shifted upward in steps of 0.06. In the lower panels the apparent magnetic field strength $B_A$ corresponding to the splitting of the Stokes $V$ peaks is indicated

constant ($B_0$ is still in the weak-field regime for such wide features). The amplitudes of the emission peaks actually decrease with $B_0$ (see below), so that in Stokes $V$ the amplitude of the absorption trough increases relative to the emission peak with increasing $B_0$. The interference of the $\sigma$-components with the absorption trough at large $B_0$ tends to move the $\sigma$-peaks closer together, thus lowering $B_A$.

The shapes of the line profiles also depend strongly on $B_0$. The vertical field strength gradient is coupled to $B_0$ and increases with it. This produces considerably broader, lower, and more asymmetric $\sigma$-components at $B_0 \gtrsim 1400$ G than at low $B_0$. To a smaller extent the interference with the absorption trough also distorts the emission peaks in both Stokes $I$ and $V$. The canceling effect and profile distortion is especially pronounced at photospheric field $B_0 = 1680$ G (see Fig. 6): if such profiles were to be observed, the broad, low amplitude $\sigma$-emission peaks would drown almost completely in the noise unless the data were of exceptional quality. At large $B_0$ each $\sigma$-component tends to be roughly triangular in shape, with a steep inner flank and a more gradual decrease in the outer part. For large $f_0$ and $B_0$ the inner "cutoff" corresponds to $B_m$, for small $f_0$ or $B_0$ to the non-magnetic width of the emission profile (weak-field limit). The wide outer flanks are a product of the large vertical field strength gradient in the flux tube below the merging height. Consequently, $B$ measured from the center of gravity of the $V$ $\sigma$-components increases more rapidly with $B_0$ than $B_A$ does. On the one hand, the interference between emission peaks and absorption trough poses severe problems to straightforward flux-tube magnetic field determinations from $\sigma$-peak separations in observed 12.32 $\mu$m line profiles, but on the other hand it offers a handle on $fB$ deeper in the photosphere, even if it is a complicated one that requires detailed modeling. Stokes $Q$ and $U$ profiles, which have absorption trough signals proportional to $B^2$, could partially solve the problem posed by emission peak/absorption trough interference.

In Paper III we found that almost all of the magnetic field detected in the Fe I 1.5648 $\mu$m line in an active region plage was concentrated into flux tubes with $B_0 = 1400 - 1700$ G, and filling factors $f_0$ ranging between 2% and 50%, with $f_0$ usually being below 15–20% (cf. Rabin 1992a, b). Our computations cover almost this whole parameter range. The synthetic 12.32 $\mu$m profiles formed in this range of magnetic features show splittings corresponding to 200 – 600 G, which agrees well with the measured splittings of 200 – 700 G (Brault & Noyes 1983; Deming et al. 1988a; Zirin & Popp 1989). Unfortunately, only Stokes $I$ was observed, which limits the accuracy of the observed splittings, in particular for weaker fields. E.g. a field with $B_0 = 500$ G, $f_0 = 16\%$ does not obviously distort Stokes $I$ (cf. Fig. 6). In Paper III, however, the presence of such fields has been demonstrated. Even Stokes $V$ does not allow such fields to be identified uniquely. For example. the 12.32 $\mu$m $V$ and $I$ profiles for $B_0 = 500$ G and $f_0 = 32\%$ are practically indistinguishable from the $V$ and $I$ profiles for $B_0 = 1000$ G and $f_0 = 16\%$. Thus for the measurement of fields that are intrinsically weak in the photosphere the 1.5648 $\mu$m line is superior to the 12 $\mu$m lines.

### *3.4. Comparison with Fe I lines*

Figure 7 compares the Stokes $V$ profiles and contribution functions of the Mg I 12.32 $\mu$m line with the $g = 3$ Fe I lines at

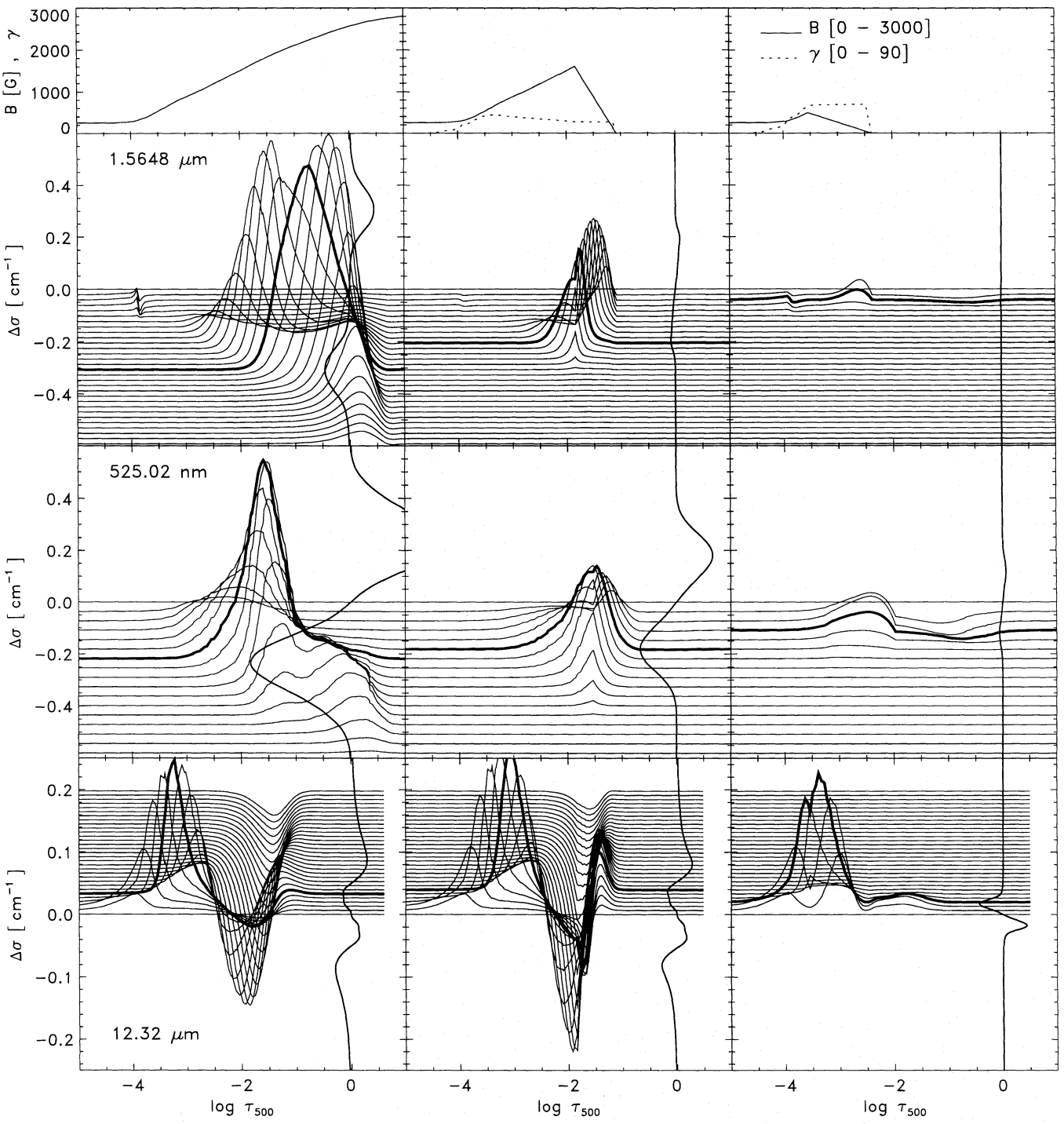


**Fig. 7.** Top row: magnetic field strength $B$ and inclination $\gamma$ ($0 - 90°$ full scale) for three representative rays (resp. 0.0, 1.0 and 1.7 tube radii from the tube axis, at $z = 0$) through the plage model PC2 with $f_0 = 16\%$ and $B_0 = 1600$ G. Next three rows: Stokes $V$ profiles and the Stokes $V$ line depression contribution functions (CFs) for lines Fe I 1.5648 $\mu$m, 525.02 nm and Mg I 12.32 $\mu$m. One $V$ profile is plotted per frame (curve running from top to bottom). The CFs at each $\Delta\sigma$ grid point, $C_{R,V}$, have first been normalized for plotting on the $\log \tau_{500}$ abscissa and then multiplied by an arbitrary factor (different for each line) and shifted vertically so that their zero level coincides with the corresponding $\Delta\sigma$ value on the ordinate. The CF curves at the $\sigma$-peak wavelengths have been drawn with thick lines. The Stokes $V$ profiles have been normalized to their respective Stokes $I$ continuum intensities: the zero-level is at $\log \tau_{500} = 0$ and the continuum-intensity spans 10 units in $\log \tau_{500}$. The $C_{R,V}$, which are anti-symmetric around line center, have been plotted for one half of the line only

525.02 nm and 1.5648 $\mu$m, obtained for three representative rays through the PC2 model with $f_0 = 16\%$ and $B_0 = 1600$ G.

The model magnetic field strength $B$ and inclination $\gamma$ are shown in the top row as a function of optical depth. From left to right the columns refer to the flux-tube axis, which has non-zero magnetic field at all heights, and to rays at increasing distance from the tube axis, so that the height where they cross the flux-tube boundary increases. The gradual (linear) decrease of $B(\log \tau_{500})$ (top row, middle and right panel) results from the interpolation onto a very fine $\log \tau_{500}$ grid across that boundary (to avoid numerical problems caused by the large opacity jump there). On a $z$ scale the change in field strength at the flux-tube boundary is very rapid; it drops to zero over approximately 10 km. The field inclination remains constant over the boundary and has no meaning in the field-free part of the atmosphere.

Rows 2–4 of Fig. 7 display the Stokes $V$ profiles and the corresponding Stokes $V$ line depression contribution function $C_{R,V}$ (Grossmann-Doerth et al. 1988; Rees et al. 1989), for the three lines in order of increasing formation height. The Stokes $V$ profiles have been normalized to the respective Stokes $I$ continuum intensities.

The line profiles in the left column are fully split ($B \approx 1.6 - 2.2$ kG for the Fe I lines and 700 G for the 12.32 $\mu$m line). The Fe I line profiles in the middle column have significantly smaller amplitude because they are partially formed in the field-free part of the atmosphere, and their splitting is smaller because strong photospheric fields are absent. Both lines are virtually insensitive to changes of the photospheric radiation fields because they are formed close to LTE. On the other hand, the 12.32 $\mu$m line is only influenced by the statistical equilibrium along this ray, which is set (in part) by the hotter photospheric radiation fields: the emission peaks are formed slightly deeper at stronger magnetic fields (larger splitting) but still completely in the magnetic part of the atmosphere. Only the infrared lines are completely split, but the 1.5648 $\mu$m line has virtually zero Stokes $V$ amplitude because it is formed largely below the magnetic region. At even larger distance from the flux-tube axis only the 12.32 $\mu$m line senses the magnetic field.

The CFs have been suitably normalized for display on the $\log \tau_{500}$ abscissa, but multiplied by an arbitrary factor (one for each line) for display on the $\Delta\sigma$ inverse wavelength ordinate of the Stokes $V$ profiles, and shifted vertically so that the zero-level of each CF curve lies at the corresponding $\Delta\sigma$ value. Thick curves indicate the CFs at the $\sigma$-peak wavelengths. The CFs in the first column are easiest to understand and clearly show the progression of the formation heights of the three lines from the deep photosphere to the upper photosphere. Note that we only consider the emission $\sigma$-peaks of the 12.32 $\mu$m line, not the absorption trough that is formed deeper in the photosphere. It is interesting to note that even for the completely split infrared lines, the CFs at the line center peak highest in the atmosphere, even though Stokes $V$ is very small at these wavelengths. This has to do with the fact that the inner point of the $V$ profile is weakly split and gets its contribution only from regions of weak field. Along the axis of our flux-tube model weak fields are present exclusively in the highest layers.

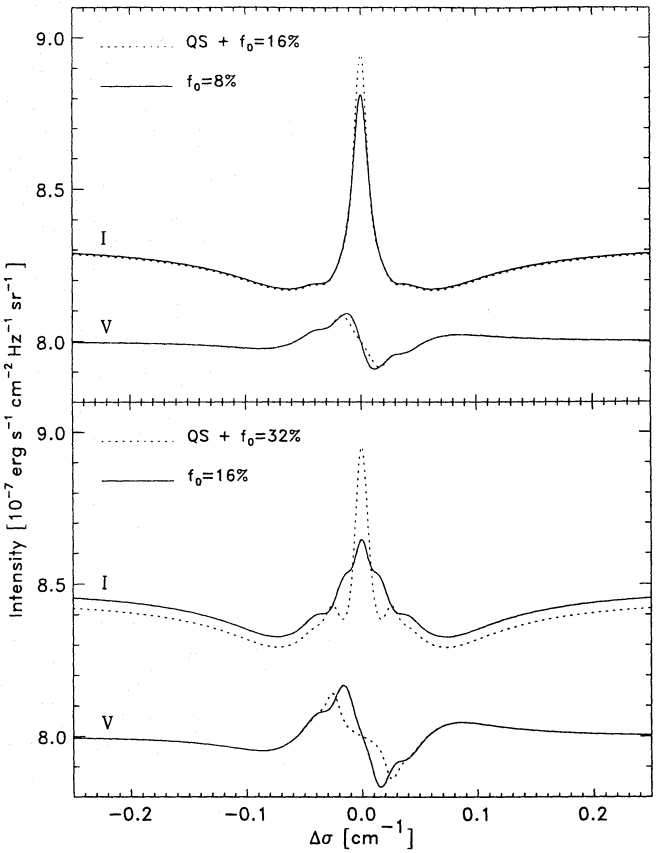


**Fig. 8.** *Top:* Mg I 12.32 $\mu$m Stokes $I$ and $V$ (shifted by arbitrary amount) profiles for model PC2 with filling factor $f_0 = 8\%$ (solid curves), compared with the line profile average (dotted curves) of the quiet-Sun model (QS) and the PC2 model with $f_0 = 16\%$, with equal weights for both models (i.e. an averaged final filling factor of 8%). *Bottom:* same as top panel, but for filling factors of 16 resp. 32%

The CFs in the next two columns show non-zero $C_{R,V}$ contribution even in the field-free deeper atmosphere, the structure of which is rather complicated when the line is not completely Zeeman split or if there is an absorption trough. Larsson et al. (1991) briefly discuss the influence on the Stokes vector CFs of the presence of magnetic and non-magnetic regions in the ray. They conclude that it is inherent to the definition of $C_{R,Q}$, $C_{R,U}$, and $C_{R,V}$ that these CFs can be non-zero in field-free regions underlying magnetic regions, whereas they should be zero in a field-free region overlying magnetic fields.

The important point to note, is that due to their different formation heights the synthetic $V$ profiles of the three lines sample different field strengths. When averaged over the flux tube with $B_0 = 1600$ G and $f_0 = 16\%$, we find $B_A \approx 2.0$ kG for the 1.5648 $\mu$m line, 1.5 kG for the 0.525 $\mu$m line and 0.35 kG for the 12.32 $\mu$m line. Smaller $B_0$ values give correspondingly smaller $B_A$. These values are in agreement with observations of the relevant spectral lines.

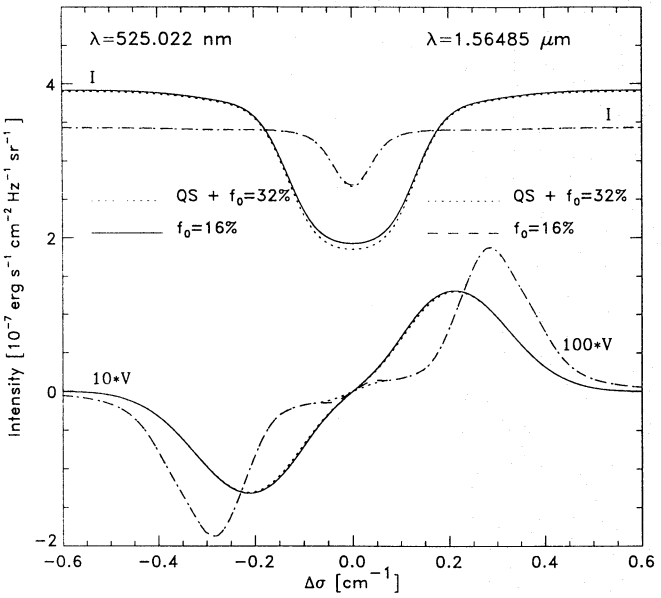


**Fig. 9.** Comparison of the Fe I 525.02 nm (solid) and 1.5648 $\mu$m (dashed) Stokes $I$ and $V$ profiles obtained from direct computation for $f_0$ = 16% and from scaling the $f_0$ = 32% results (dotted for both lines)

### *3.5. Scaling of line profiles*

Scaling of the computed Stokes $V$ amplitude to determine filling factors is common practice for flux-tube analyses using visible and near-infrared lines. For this procedure to be valid the lines should not have knowledge of the merging height, or they should be only weakly split. The 12.32 $\mu$m line fulfills neither of these conditions.

Already from Fig. 5 it is evident that there is no simple scaling relation that translates 12.32 $\mu$m line profiles from one $f_0$ value to another, since the line profile shape changes strongly along the sequence of $f_0$ values. Figure 8 more clearly demonstrates that scaling of line profiles is not a valid procedure for the 12.32 $\mu$m line, especially not when the magnetic filling factor is large. The upper panel of this figure shows the Stokes $I$ and $V$ profiles for model PC2 with $f_0$ = 8% (solid), and compares them with the profiles that result from averaging, with equal weights, the profiles for model PC2 with $f_0$ = 16% and for the quiet-Sun (dotted). The dotted profile thus also corresponds to an average filling factor of 8%. At this filling factor combination the profile differences become apparent, particularly near line center. At lower filling factors (roughly $f_0 < 8\%$) the Stokes $I$ and $V$ profile shapes do not depend strongly on $f_0$, and the profile scaling method works well. At larger filling factors, however, the discrepancies are striking (Fig. 8, lower panel). Consequently it is impossible to scale the Mg I 12.32 $\mu$m line profiles for one value of $f_0$ to get profiles for another $f_0$, except at low $f_0$. Therefore the filling factor, flux-tube expansion and merging need to be incorporated explicitly in a 12.32 $\mu$m line flux-tube analysis. Outside of sunspots the modeling of the 12.32 $\mu$m line by means of a magnetic and a non-magnetic component with height-independent filling factors $f$ and $1 - f$ is not to be recommended.

More important is that the dependence of the line profile shape on $f_0$ leads to a large variety of shapes if we assume that plage flux tubes are distributed relatively randomly. This may explain the diversity of observed line shapes (e.g. Zirin & Popp 1989). Note that by combining profiles produced by flux tubes with different $B_0$ and $f_0$ a much larger range of profile shapes can be produced than we have shown. Such distributions of field strength and filling factor are expected to be present in the 4–10″ apertures used for the observations.[2]

A comparison similar to that shown in Fig. 8, for the Fe I lines at 525.02 nm and 1.5648 $\mu$m demonstrates that they may easily be scaled to simulate different filling factors. For example, the $f_0$ = 16% profile obtained by scaling the $f_0$ = 32% profile coincides very well with the consistently computed $f_0$ = 16% profile (Fig. 9). Comparing Fig. 9 with 8 shows the major difference between the Fe I and Mg I lines. The property of the Mg I line that it does not scale with filling factor for typical plage $f_0$ values, is, to our knowledge, unique.

## 4. Discussion and conclusion

We have studied the behavior of the 12.32 $\mu$m line under conditions characteristic of solar plage. As shown already in Paper VIII for constant energy-flux models of different effective temperature, the line emission strength depends on the assumed photospheric temperature (mainly a Saha-Boltzmann population effect). For the range of photospheric temperature stratifications considered here, which are representative of plage and network, the line profile shape is largely preserved. Similarly, for different choices of the chromospheric temperature rise the line profile changes only moderately. Only if the chromospheric temperature rise occurs very deep in the atmosphere does it lead to significantly smaller emission peaks. Such a deep-lying chromosphere is unlikely (Bruls & Solanki 1993). The low temperature sensitivity of the 12.32 $\mu$m line adds to its potential as a magnetic field diagnostic.

The large Zeeman separation of the emission $\sigma$-peaks in principle enables accurate upper photosphere magnetic field measurements down to a few hundred Gauss. In practice we find that the splitting of the synthetic line profiles resulting from flux-tube models, which consistently include the main features of the magnetic field, depends not only on the magnetic field strength, but also on the filling factor (via the merging height). On the one hand this complicates the analysis of the Mg I 12 $\mu$m emission lines observed in plages, which consequently need to be analyzed using detailed models. Thus, to reproduce the often complex profile shapes observed in solar plage it may well be necessary to use multiple magnetic components, which not only differ in field strength, but also in local density of flux tubes (filling factor). On the other hand, this very property of the 12 $\mu$m

[2] A relatively random spatial distribution of flux tubes is suggested by the relation between Ca II K core emission and magnetic flux (Schrijver 1993).

lines means that they can provide some information on the inhomogeneity of the distribution of flux tubes within the resolution element. In this respect these lines constitute a unique diagnostic. They also provide observational evidence for the merging height of flux tubes in strong plages. We believe that the diagnostic potential of these lines will be enhanced considerably if they are observed and studied in conjunction with the $g = 3$ Fe I line at 1.5648 $\mu$m. This infrared line, which is formed deeper in the photosphere, can disentangle different field strengths present in the resolution element. Using this information, it may then be possible to obtain the distribution of filling factors, or the clumpiness of the distribution of the magnetic flux tubes from the 12.32 $\mu$m line.

The large and complex dependence of line shape and splitting on the intrinsic field strength and filling factor of small-scale magnetic features also means that the typical difference in $B_0$ and $f_0$ present between different plages and different positions within a plage, completely dominate over any dependence of the splitting on the limb distance. Thus it is not surprising that Zirin & Popp (1989) did not find any such dependence, although they did see profiles of many different shapes.

The brief qualitative comparison with observations which we have carried out, suggests that the basic description of small-scale magnetic features using flux tubes is correct. In particular, we find that the thin-tube approximation extended to include the merging with neighboring flux tubes, is an adequate representation. Not only does such a model simultaneously reproduce the observed splitting of Zeeman-sensitive lines formed in the deep (1.5648 $\mu$m), middle (525.02 nm) and upper (12.32 $\mu$m) photosphere, it also predicts the presence of a large variety of different profile shapes of the 12 $\mu$m emission lines, as observed by Zirin & Popp (1989).

Note that in plages close to sunspots the profile shapes may be even more strongly distorted than our computations suggest due to the presence of the sunspot canopy in addition to the flux tubes. In Paper VIII we showed that this canopy strongly affects the 12.32 $\mu$m line. The simultaneous presence of a sunspot canopy and small flux tubes has been deduced from spectra of Fe I 1.5648 $\mu$m (Solanki et al. 1992b, Paper V). Observed 12.32 $\mu$m Stokes $V$ profiles, not available yet for plages, would enhance our knowledge about plage flux tubes considerably, since they contain information almost exclusively about the magnetic parts of the atmosphere, whereas Stokes $I$ profiles contain significant non-magnetic contributions (e.g. part of its line-center emission peak). For flux tubes, however, which have large photospheric field strengths, magnetic field measurements with the 12.32 $\mu$m may be difficult to interpret even with Stokes $V$ information, due to the complex profile shapes, especially at larger field strengths and filling factors. The Stokes $Q$ and $U$ profiles, which have much smaller absorption trough signals, could solve part of the problem.

*Acknowledgements.* We thank M. Carlsson, R.J. Rutten and N.G. Shchukina for making available the Mg model atom.

## References


Anders E., Grevesse N., 1989, Geochim. Cosmochim. Acta 53, 197

Auer L. H., Heasley J. N., Milkey R. W., 1972, A Computational Method for the Solution of Non-LTE Transfer Problems by the Complete Linearization Method, Contribution No. 555, Kitt Peak National Observatory

Ayres T. R., Testerman L., Brault J. W., 1986, ApJ 304, 542

Brault J., Noyes R., 1983, ApJ 269, L61

Bruls J. H. M. J., 1992, Formation of diagnostic lines in the solar spectrum, PhD Thesis, Rijksuniversiteit Utrecht, Utrecht

Bruls J. H. M. J., Solanki S. K., 1993, A&A 273, 293

Bruls J. H. M. J., Solanki S. K., Rutten R. J., Carlsson M., 1994, A&A this issue (Paper VIII)

Carlsson M., 1986, A Computer Program for Solving Multi-Level Non-LTE Radiative Transfer Problems in Moving or Static Atmospheres, Report No. 33, Uppsala Astronomical Observatory

Carlsson M., Rutten R. J., Shchukina N. G., 1992, A&A 253, 567

Chang E. S., 1987, Physica Scripta 35, 792

Chapman G. A., 1979, ApJ 232, 923

Defouw R. J., 1976, ApJ 209, 266

Deming D., Boyle R. J., Jennings D. E., Wiedemann G., 1988a, ApJ 333, 978

Deming D., Glenar D. A., Käufl H. U., Espenak F., 1988b, in J. Christensen-Dalsgaard, S. Frandsen (eds.), Advances in Helio- and Asteroseismology, IAU Symposium 123 (Aarhus), Kluwer, Dordrecht, p. 425

Deming D., Hewagama T., Jennings D. E., Osherovich V., Wiedemann G., 1990, ApJ 364, L49

Fuhr J. R., Martin G. A., Wiese W. L., 1988, J. Phys. Chem. Ref. Data 17, Suppl. 4

Gigas D., 1986, A&A 165, 170

Grossmann-Doerth U., Larsson B., Solanki S. K., 1988, A&A 204, 266

Hewagama T., 1991, An infrared polarimetric study of sunspots, Ph.D. Thesis, University of Maryland, College Park, Maryland

Hewagama T., Deming D., Jennings D. E., Osherovich V., Wiedemann G., Zipoy D., Mickey D. L., Garcia H., 1993, ApJS 86, 313

Keller C. U., Solanki S. K., Steiner O., Stenflo J. O., 1990, A&A 233, 583

Knölker M., Schüssler M., 1988, A&A 202, 275

Larsson B., Solanki S. K., Grossmann-Doerth U., 1991, in L. J. November (ed.), Solar Polarimetry, Proc. 11th NSO/SP Summer Workshop, National Solar Observatory, Sunspot, New Mexico, p. 479

Maltby P., Avrett E. H., Carlsson M., Kjeldseth-Moe O., Kurucz R. L., Loeser R., 1986, ApJ 306, 284

Mathisen R., 1984, Oslo Inst. Theor. Astrophys. Publ. Series 1, 1

Murphy G. A., 1990, The Synthesis and Inversion of Stokes Spectral Profiles, NCAR Cooperative Thesis No. 124, High Altitude Observatory, Boulder

Murphy G. A., Rees D. E., 1990, Operation of the Stokes Profile Synthesis Routine, NCAR Technical Note NCAR/TN-348+IA, High Altitude Observatory, Boulder

Olson G. L., Auer L. H., Buchler J. R., 1986, J. Quant. Spectrosc. Radiat. Transfer 35, 431

Rabin D., 1992a, ApJ 390, L103

Rabin D., 1992b, ApJ 391, 832

Rees D. E., 1969, Solar Phys. 10, 268

Rees D. E., 1987, in W. Kalkofen (ed.), Numerical Radiative Transfer, Cambridge University Press, Cambridge, Great Britain, p. 213

Rees D. E., Murphy G. A., Durrant C. J., 1989, ApJ 339, 1093
Rüedi I., Solanki S. K., Livingston B., Stenflo J. O., 1992, A&A 263, 323 (Paper III)
Schrijver C. J., 1993, A&A 269, 395
Schüssler M., 1986, in W. Deinzer, M. Knölker, H. H. Voigt (eds.), Small Scale Magnetic Flux Concentrations in the Solar Photosphere, Abhandl. Akad. Wiss. Göttingen, Math.-Phys. Klasse Dritte Folge Nr. 38, Vandenhoeck und Ruprecht, Göttingen, 103
Solanki S. K., 1986, A&A 168, 311
Solanki S. K., Brigljević V., 1992, A&A 262, L29
Solanki S. K., Roberts B., 1992, MNRAS 256, 13
Solanki S. K., Steenbock W., 1988, A&A 189, 243
Solanki S. K., Steiner O., 1990, A&A 234, 519
Solanki S. K., Steiner O., Uitenbroek H., 1991, A&A 250, 220
Solanki S. K., Rüedi I., Livingston W., 1992a, A&A 263, 312 (Paper II)
Solanki S. K., Rüedi I., Livingston W., 1992b, A&A 263, 339 (Paper V)
Steiner O., Pizzo V. J., 1989, A&A 211, 447
Stenholm L. G., Stenflo J. O., 1977, A&A 58, 273
Stenholm L. G., Stenflo J. O., 1978, A&A 67, 33
Walton S. R., 1987, ApJ 312, 909
Watanabe T., Steenbock W., 1986, A&A 165, 163
Zayer I., Solanki S. K., Stenflo J. O., 1989, A&A 211, 463
Zirin H., Popp B., 1989, ApJ 340, 571

This article was processed by the author using Springer-Verlag LaTeX A&A style file version 3.